IMAGING

Multimodal imaging of bacterial-host interface in mice and piglets with *Staphylococcus aureus* endocarditis

Peter Panizzi[1]*†, Marvin Krohn-Grimberghe[2,3]*, Edmund Keliher[2], Yu-Xiang Ye[2], Jana Grune[2], Vanessa Frodermann[2], Yuan Sun[2], Charlotte G. Muse[1], Kaitlyn Bushey[4], Yoshiko Iwamoto[2], Mandy M. T. van Leent[5], Anu Meerwaldt[5], Yohana C. Toner[5], Jazz Munitz[5], Alexander Maier[5], Georgios Soultanidis[5], Claudia Calcagno[5], Carlos Pérez-Medina[5,6], Giuseppe Carlucci[7], Kay P. Riddell[8], Sharron Barney[9], Glenn Horne[9], Brian Anderson[10], Ashoka Maddur-Appajaiah[11], Ingrid M. Verhamme[11], Paul E. Bock[11‡], Gregory R. Wojtkiewicz[2], Gabriel Courties[2], Filip K. Swirski[2], William R. Church[4], Paul H. Walz[8], D. Michael Tillson[9], Willem J. M. Mulder[5,12,13], Matthias Nahrendorf[2,14,15†§]

Acute bacterial endocarditis is a rapid, difficult to manage, and frequently lethal disease. Potent antibiotics often cannot efficiently kill *Staphylococcus aureus* that colonizes the heart's valves. *S. aureus* relies on virulence factors to evade therapeutics and the host's immune response, usurping the host's clotting system by activating circulating prothrombin with staphylocoagulase and von Willebrand factor–binding protein. An insoluble fibrin barrier then forms around the bacterial colony, shielding the pathogen from immune cell clearance. Targeting virulence factors may provide previously unidentified avenues to better diagnose and treat endocarditis. To tap into this unused therapeutic opportunity, we codeveloped therapeutics and multimodal molecular imaging to probe the host-pathogen interface. We introduced and validated a family of small-molecule optical and positron emission tomography (PET) reporters targeting active thrombin in the fibrin-rich environment of bacterial colonies. The imaging agents, based on the clinical thrombin inhibitor dabigatran, are bound to heart valve vegetations in mice. Using optical imaging, we monitored therapy with antibodies neutralizing staphylocoagulase and von Willebrand factor–binding protein in mice with *S. aureus* endocarditis. This treatment deactivated bacterial defenses against innate immune cells, decreased in vivo imaging signal, and improved survival. Aortic or tricuspid *S. aureus* endocarditis in piglets was also successfully imaged with clinical PET/magnetic resonance imaging. Our data map a route toward adjuvant immunotherapy for endocarditis and provide efficient tools to monitor this drug class for infectious diseases.

INTRODUCTION

Bacterial endocarditis is an often lethal infection of the heart valves and surrounding endocardium (*1*). Major challenges to clinically managing endocarditis include identifying the causal pathogens, timing surgical interventions, and rising bacterial resistance to antibiotics (*2*). To address these difficulties, we here introduce imaging tools for fundamental and translational research examining host-pathogen interactions.

Staphylococcus aureus is the most common cause of acute endocarditis in patients (*1*), likely because these bacteria produce potent factors promoting bacterial virulence and survival. Historically, *S. aureus* has been differentiated from other pathogens, such as *Staphylococcus epidermidis*, through its distinct ability to clot blood (*3*). This directly results from *S. aureus*' production of the two redundant prothrombin activators staphylocoagulase (SC) and von Willebrand factor–binding protein (vWBp) (*4*, *5*). SC and vWBp both bind active prothrombin through N-terminal interactions and stay locked into the vegetation through independent C-terminal binding interactions. This anchoring mechanism essentially paints vegetations with layers of thrombin-like proteolytic activity (*6*, *7*). As a consequence, a fibrin-rich wall shields the bacterial colony against drugs and immune cells.

The coagulase-prothrombin complex binds direct thrombin inhibitors such as dabigatran (DAB) (*8*). Here, we introduce a family of DAB-derived small-molecule imaging agents that target the SC-(pro)thrombin or vWBp-(pro)thrombin complexes residing in growing *S. aureus* vegetations. The radioisotope twin of this imaging agent family has the potential to monitor *S. aureus* endocarditis in large animals, whereas the fluorescent sibling enables intravital microscopy and fluorescence molecular tomography (FMT) in mice. Such DAB analogs should be useful imaging agents given their low toxicity profile, small size, short blood half-life, and high tissue permeability.

[1]Department of Drug Discovery and Development, Harrison School of Pharmacy, Auburn University, Auburn, AL 36849, USA. [2]Center for Systems Biology and Department of Radiology, Massachusetts General Hospital Research Institute, Harvard Medical School, Boston, MA 02114, USA. [3]University Heart Center Freiburg, 79106 Freiburg, Germany. [4]Green Mountain Antibodies, Burlington, VT 05401, USA. [5]Biomedical Engineering and Imaging Institute, Department of Radiology, Icahn School of Medicine at Mount Sinai, New York, NY 10029, USA. [6]Centro Nacional de Investigaciones Cardivasculares, 28029 Madrid, Spain. [7]Bernard and Irene Schwarz Center for Biomedical Imaging, New York University, New York, NY 10016, USA. [8]Department of Pathobiology, College of Veterinary Medicine, Auburn University, Auburn, AL 36849, USA. [9]Department of Clinical Science, College of Veterinary Medicine, Auburn University, Auburn, AL 36849, USA. [10]Swine Research and Education Center, Department of Animal Sciences, Auburn University, Auburn, AL 36849, USA. [11]Department of Pathology, Microbiology and Immunology, Vanderbilt University Medical Center, Nashville, TN 37212, USA. [12]Department of Oncological Sciences, Icahn School of Medicine at Mount Sinai, New York, NY 10029, USA. [13]Laboratory of Chemical Biology, Department of Biomedical Engineering and Institute for Complex Molecular Systems, Eindhoven University of Technology, 5612 AZ Eindhoven, Netherlands [14]Cardiovascular Research Center, Massachusetts General Hospital, Harvard Medical School, Boston, MA 02114, USA. [15]Department of Internal Medicine I, University Hospital Würzburg, 97080 Würzburg, Germany.
*These authors contributed equally to this work.
†These authors jointly supervised this work.
‡Deceased.
§Corresponding author. Email: mnahrendorf@mgh.harvard.edu

We therefore (i) synthesized and characterized DAB derivates labeled with either a near-infrared fluorochrome or the positron emission tomography (PET) isotope fluorine-18, (ii) used the fluorescent imaging agent in noninvasive fluorescence tomography and intravital microscopy to assess the relative distribution of thrombin activity in growing vegetations, (iii) developed a piglet model of tricuspid *S. aureus* endocarditis, (iv) demonstrated the feasibility of integrated PET/magnetic resonance imaging (MRI) for detecting of *S. aureus* endocarditis using ^{18}F-DAB in mice and piglets, and (v) evaluated by imaging an immunotherapy that neutralizes SC and vWBp in mice with endocarditis. This therapy reduced thrombin deposition, boosted innate immune cell defense, and impeded vegetation formation. Ultimately, our work furthers the development of PET imaging agents for diagnosing *S. aureus* endocarditis and provides a facile preclinical tool to accelerate the discovery of antimicrobial compounds and therapies adjunctive to antibiotics.

RESULTS

Synthesizing imaging agents ^{18}F-DAB and DAB–VivoTag 680XL

Thrombin activation through *S. aureus* virulence factors is a key bacterial defense mechanism downstream of potential drug targets. A targeted imaging agent thus has the potential to aid first preclinical discovery and later therapeutic trials. We therefore developed an imaging agent based on the Food and Drug Administration (FDA)–approved thrombin inhibitor DAB, capitalizing on the high affinity and specificity of this small-molecule inhibitor. We synthesized both fluorescent and radioactively labeled versions in two steps (Fig. 1A). First, we derivatized DAB with an amino group. The DAB-amino intermediate was then used to attach either the radioisotope fluorine-18 (^{18}F), to yield the PET imaging agent ^{18}F-DAB, or the fluorochrome VivoTag 680XL (VT680XL), to synthesize the near-infrared imaging agent DAB-VT680XL, which can be used for intravital microscopy and FMT. Mass spectrometry (MS) after liquid chromatography (LC) confirmed the identities of DAB-VT680XL (Fig. 1B) and the nonradioactive standard ^{19}F-DAB (Fig. 1C). Note that ^{18}F-DAB has a specific collection window (Fig. 1D) to obtain the imaging agent with high radiochemical purity (Fig. 1, E and F).

As expected, ^{19}F-DAB's affinity for thrombin was less than the drugs argatroban and DAB (Fig. 1G); however, it remained sufficient for use as a sensitive imaging agent. Serial blood sampling after intravenous ^{18}F-DAB injection into mice yielded a short blood half-life of 2.0 ± 0.6 min, which is typical for small-molecule imaging agents that are rapidly renally eliminated (Fig. 1H). Such fast clearance is advantageous for imaging endocarditis vegetations, which are surrounded by the blood. Biodistribution studies of ^{18}F-DAB in mice documented low uptake in the normal heart and vasculature (Fig. 1I).

DAB-VT680XL binds to endocarditic vegetations

After establishing the chemical and kinetic properties of the two DAB-based imaging agents, we next investigated the in vivo binding of DAB-VT680XL to arterial thrombi. We induced thrombosis in the femoral artery of mice by placing a ferric chloride–soaked filter paper on the exposed artery. Using intravital microscopy and platelet visualization by injecting a fluorescently labeled antibody binding CD41, we detected DAB-VT680XL in the thrombus (Fig. 2A), whereas a control VT680XL compound (Gly-VT680XL) did not show any binding (Fig. 2B).

To test whether DAB-VT680XL binds to vegetations, we induced *S. aureus* endocarditis in mice using a combination of suture insertion and intravenous injection of bacteria, as described previously (*7*), and injected 2 nmol of DAB-VT680XL 90 min before euthanasia. Vegetations and valve involvement were accessed by Gram staining (Fig. 3, A and B). On an adjacent tissue section, DAB-VT680XL visualized the typically fibrin-rich wall (*9*) that surrounds bacterial vegetation (Fig. 3, C to G). Costaining for CD11b$^+$ innate immune cells indicates that the DAB-VT680XL–positive vegetation barrier shields bacteria from the host immune response, as myeloid cells assembled in the vascular wall in front of this barrier but were unable to cross it into the bacterial colony (Fig. 3, D and G).

Noninvasively imaging *S. aureus* endocarditis in mice

Because of light waves' poor penetration depth in tissue, optical imaging is unsuitable for imaging deep tissues. We therefore developed companion fluorescent and PET imaging agents and deployed them for fluorescence molecular (DAB-VT680XL; Fig. 4, A to E) and PET (^{18}F-DAB; Fig. 4, F to J), respectively. FMT/x-ray computed tomography (FMT/CT) data demonstrated high DAB-VT680XL concentration in the aortic roots of mice with endocarditis (Fig. 4, A and B), whereas some signal was also observed in more distal vasculature along the suture inserted to induce endocarditis, likely due to bacteria colonizing the foreign material. Ex vivo fluorescence imaging of the excised aorta colocalized DAB-VT680XL signal with bioluminescent signal from Xen29 *S. aureus* (Fig. 4C). In sham-operated control mice that were also injected with DAB-VT680XL, fluorescent background was much lower than in mice with endocarditis (Fig. 4D), whereas bioluminescence signal was absent (Fig. 4E). A blocking experiment with 100-fold excess intravenous injection of DAB preceding injection of the imaging probe DAB-VT680XL confirmed specificity of binding (fig. S1). We observed no DAB-VT680XL enrichment in FMT/CT imaging of mice with myocardial infarction, a setting of sterile inflammation (fig. S2). If endocarditis was induced with *S. epidermidis* Xen43, then the FMT/CT signal obtained from lesions was lower than with *S. aureus* Xen29 (fig. S3). PET/CT imaging after ^{18}F-DAB injection indicated binding of the PET isotope-labeled imaging agent to endocarditis vegetations (Fig. 4, F and G). Ex vivo scintillation counting of aortas confirmed high ^{18}F-DAB uptake (Fig. 4H), which colocalized on autoradiography with bacteria-derived bioluminescent signal (Fig. 4, I and J). To explore the utility of this imaging approach in other sites of infection, we imaged mice that developed renal *S. aureus* lesions. Twenty-four hours after injection, we observed DAB-VT680XL accumulated in infected kidneys (fig. S4).

S. aureus endocarditis in piglets

Ideally, molecular imaging probes that show satisfactory performance in mice are next tested in a large animal model. This step enables testing the approach using clinical imaging equipment. Perhaps even more importantly, host defense processes differ considerably between mice and large animals or humans. We used two piglet models of acute *S. aureus* endocarditis: one affecting the tricuspid valve and the other affecting the aortic valve. To mimic the typical pathogenesis of right heart endocarditis in patients, we subcutaneously implanted a vascular port into newly weaned piglets, inserting the central line into the right external jugular vein. The central line was then advanced via the superior vena cava into the right ventricle under fluoroscopy guidance. Six hours after implantation, we injected 4×10^8 to 8×10^8 colony forming units (CFU) of bioluminescent *S. aureus* into the

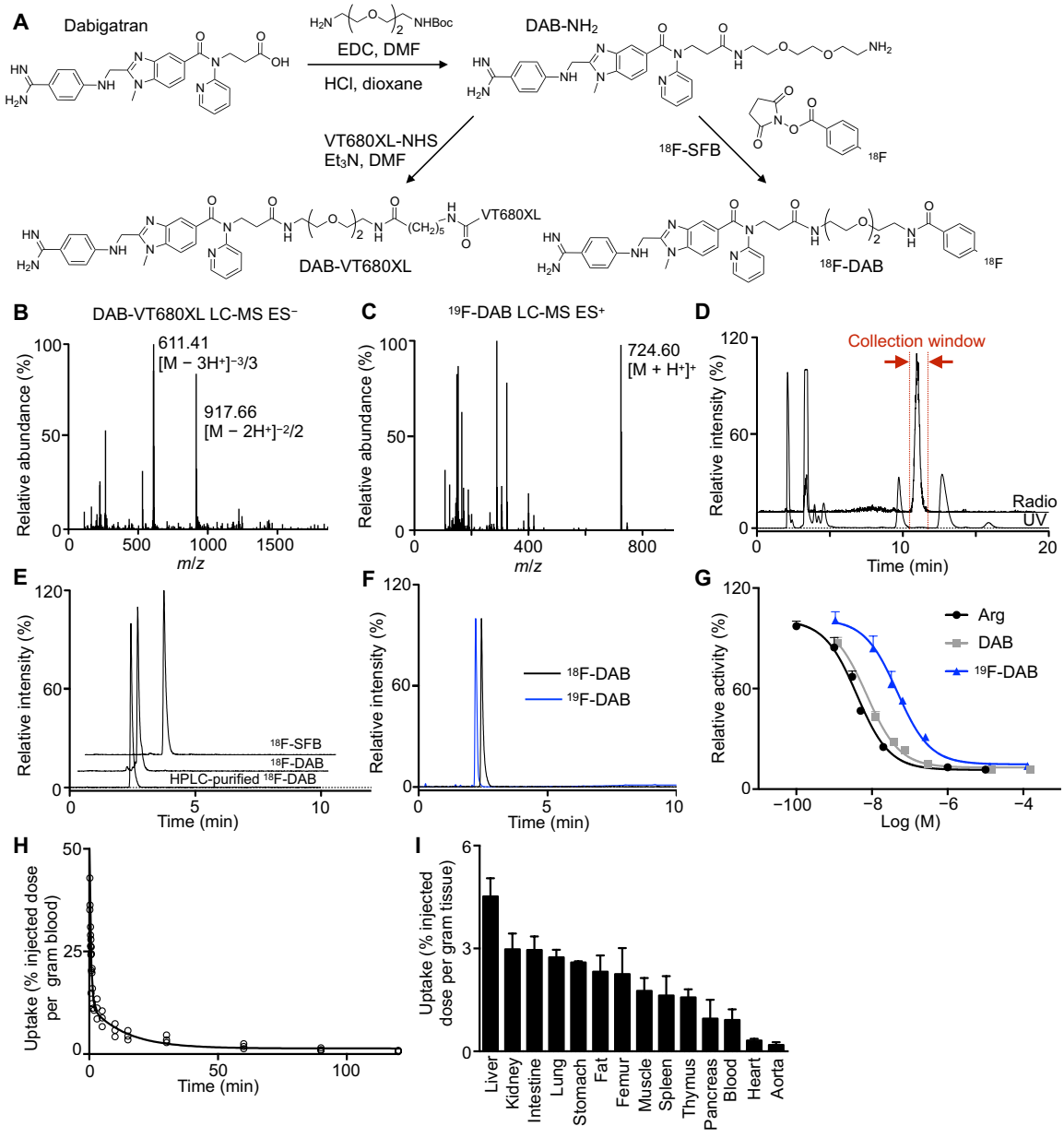

Fig. 1. Imaging agent synthesis and validation. (**A**) Synthesis scheme of a near-infrared fluorescent dabigatran derivative (DAB-VT680XL) and a positron emission tomography fluorine-18 tracer ^{18}F-dabigatran (^{18}F-DAB), both prepared in two steps from DAB. (**B**) LC-MS analysis of DAB-VT680XL showing the $[M - 2H^+]^{2-}/2$ (917.66 *m/z*) and $[M - 3H^+]^{3-}/3$ (611.41 *m/z*) ions and (**C**) ^{19}F-DAB showing the $[M + H^+]^+$ (724.60 *m/z*). (**D**) Preparative HPLC chromatograms (radio; top trace) and ultraviolet (UV) absorbance at 254 nm (bottom trace). The collection window is highlighted in red. (**E**) Analytical HPLC chromatograms of the ^{18}F–succinimidyl fluorobenzoate (^{18}F-SFB) prosthetic group, ^{18}F-DAB crude conjugation reaction mixture and HPLC-purified ^{18}F-DAB. (**F**) Analytical HPLC chromatograms of ^{18}F-DAB and stable-isotope standard ^{19}F-DAB (blue). Because the two detectors are connected in series, there is a 0.2-min delay between UV and radio signals. (**G**) Thrombin activity assay with argatroban (Arg), DAB, and ^{19}F-DAB. (**H**) Clearing ^{18}F-DAB from mouse blood ($n = 3$). The half-life in the blood is 2.0 ± 0.6 min. (**I**) Biodistribution of ^{18}F-DAB in mice ($n = 3$ to 8). Data are shown as means ± SEM.

port. Over the course of 10 days, piglets developed typical clinical signs of endocarditis, including fever (39.7 to 41.4°C) and heart murmurs. Bacteria presence on the porcine tricuspid valve was verified by hematoxylin and eosin (H&E) staining (Fig. 5A), and staphylococcal cells were identified by Gram staining (Fig. 5B).

We subsequently characterized this *S. aureus* endocarditis piglet model by clinical cardiac MRI on a 3-T human scanner. We observed the development of two to four differently sized tricuspid endocarditis lesions in the right ventricles of piglets on days 10 and 11 after bacterial injection (Fig. 5C and movies S1 and S2). Autopsy confirmed endocarditis vegetations, the morphology of which was reminiscent of those typically found in patients (Fig. 5D). Further, administering fluorescent DAB-VT680XL into the piglets' ear veins allowed visualization of endocarditis vegetations, as the probe's fluorescent signal colocalized with bacterial bioluminescence (Fig. 5, E to H).

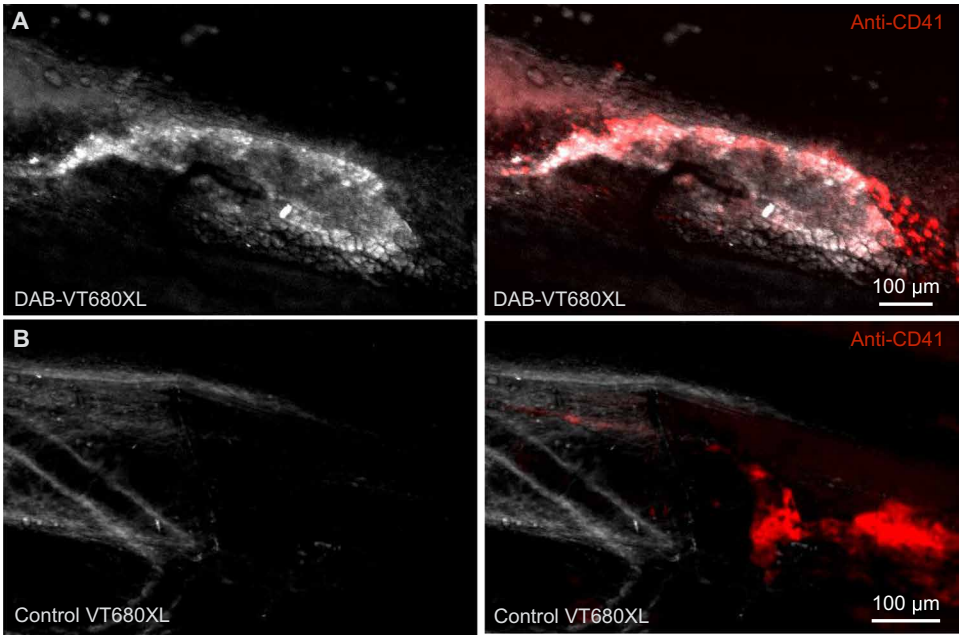

Fig. 2. In vivo DAB-VT680XL or control probe binding to thrombi in mice. (**A**) Intravital microscopy of a $FeCl_3$-induced thrombosis of the femoral artery 90 min after injection of DAB-VT680XL or (**B**) an unspecific control fluorochrome (VT680XL). Aggregating platelets are stained with anti-CD41 monoclonal antibody (red). The experiments were repeated twice with the same result ($n = 3$ per group).

For induction of left-sided endocarditis, the aortic valve was damaged with a cytology brush after gaining vascular access via the carotid artery, followed by intravenous injection of 5×10^8 to 8×10^8 CFU of bioluminescent *S. aureus*. Piglets with left-sided endocarditis deteriorated clinically faster than piglets with right-sided endocarditis. We therefore imaged them on day 7 after disease induction. Cardiac MRI revealed the development of aortic valve lesions (Fig. 5, I and J). Volumetric assessment of piglet hearts with right- and left-sided endocarditis indicated that the right ventricular ejection fraction was lower in piglets with tricuspid disease (Fig. 5K). Ex vivo bioluminescence signal colocalized with lesions on autopsy, which enriched DAB-VT680XL after intravenous injection (Fig. 5, L to P).

Encouraged by the PET data obtained in mice and optical DAB-VT680XL signal in piglets with endocarditis, we initiated a proof-of-concept PET/MRI study, a step typically taken if a molecular imaging probe performs as desired in small animals. To that aim, we developed an integrated PET/MRI cardiac imaging protocol on a clinical scanner to simultaneously acquire high-resolution morphological information and radiotracer distribution in piglet hearts. We injected the PET imaging probe ^{18}F-DAB into three piglets with left- or right-sided endocarditis, respectively. PET/MRI revealed focal enrichment of the PET imaging agent in the aortic (Fig. 6, A and B) and tricuspid valves (Fig. 6, C and D). Autoradiographic ^{18}F-DAB signal colocalized with bacterial bioluminescence arising from vegetations (Fig. 6, E to G). Together, these data indicate that combining molecular PET imaging with cardiac MRI's soft tissue contrast, anatomic detail and functional capabilities may provide complementary diagnostic information to monitor and manage endocarditis.

We proceeded to compare the fluorescence in aortic versus tricuspid vegetations of piglets injected with DAB-VT680XL. We found that the target-to-background ratio was higher in aortic valve vegetations when compared to tricuspid disease (fig. S5A), which was matched by the higher bioluminescence signal in aortic lesions (fig. S5B). This difference in imaging signal may relate to bacterial load, supported by a positive correlation between bacterial bioluminescence signal and DAB-VT680XL binding across vegetations examined in both valves (fig. S5C). We speculate that these differences may have been caused by the faster clinical disease progression and the earlier imaging time point in piglets with left-sided endocarditis.

Antibody immunotherapy disrupts vegetation anatomy and improves mouse survival

SC and vWBp are virulence factors that *S. aureus* uses to activate the clotting cascade. The resulting fibrin wall protects bacterial colonies from the host's immune system (*7*). We thus hypothesized that combined antibody–mediated inhibition of these two factors would disrupt *S. aureus*' ability to form fortified vegetations. Monoclonal antibodies raised against NH_2-terminal peptides of SC (GMA-2105) and vWBp (GMA-2150), which we engineered in mice, were tested for specificity by immunoblotting. The Western blot data indicate excellent specificity and no cross-reactivity of the GMA-2105 antibody with vWBp or cross-reactivity of GMA-2510 with SC (Fig. 7, A to C). Clotting assays demonstrated that targeted antibodies reduce fibrinogen conversion to fibrin in a concentration-dependent manner for both anti-SC and anti-vWBp therapies (Fig. 7, D and E). Treating mice with these monoclonal antibodies led to reduced DAB-VT680XL signal in FMT/CT imaging (Fig. 7, F and G), thereby indicating that therapeutically inhibiting SC and vWBp reduces active thrombin in bacterial colonies. Injecting neutralizing antibodies improved the survival of mice with endocarditis (Fig. 7H).

To explore how this treatment acts mechanistically, we imaged vegetations using DAB-VT680XL and intravital microscopy. The heart valves in living mice are difficult to approach with a microscope objective. We therefore established *S. aureus* vegetations in the femoral artery by inserting a suture and then intravenously injecting *S. aureus* expressing red fluorescent protein (RFP). This formed femoral artery vegetations that were comparable to the anatomy observed in the aortic valves of mice (Fig. 7, I and J). Specifically, we observed a central RFP^+ bacterial colony surrounded by DAB-VT680XL signal highlighting a thrombin-rich layer (Fig. 7J). Staining neutrophils with intravenously injected fluorescent antibody targeting Ly-6G indicated that neutrophils were unable to penetrate the capsule around RFP^+ bacteria (movie S3). Treatment with antibodies neutralizing SC and vWBp disrupted the DAB-VT680XL–stained capsule around RFP^+ bacteria, thereby granting neutrophils access to invade the *S. aureus* colony (Fig. 7I and movie S4).

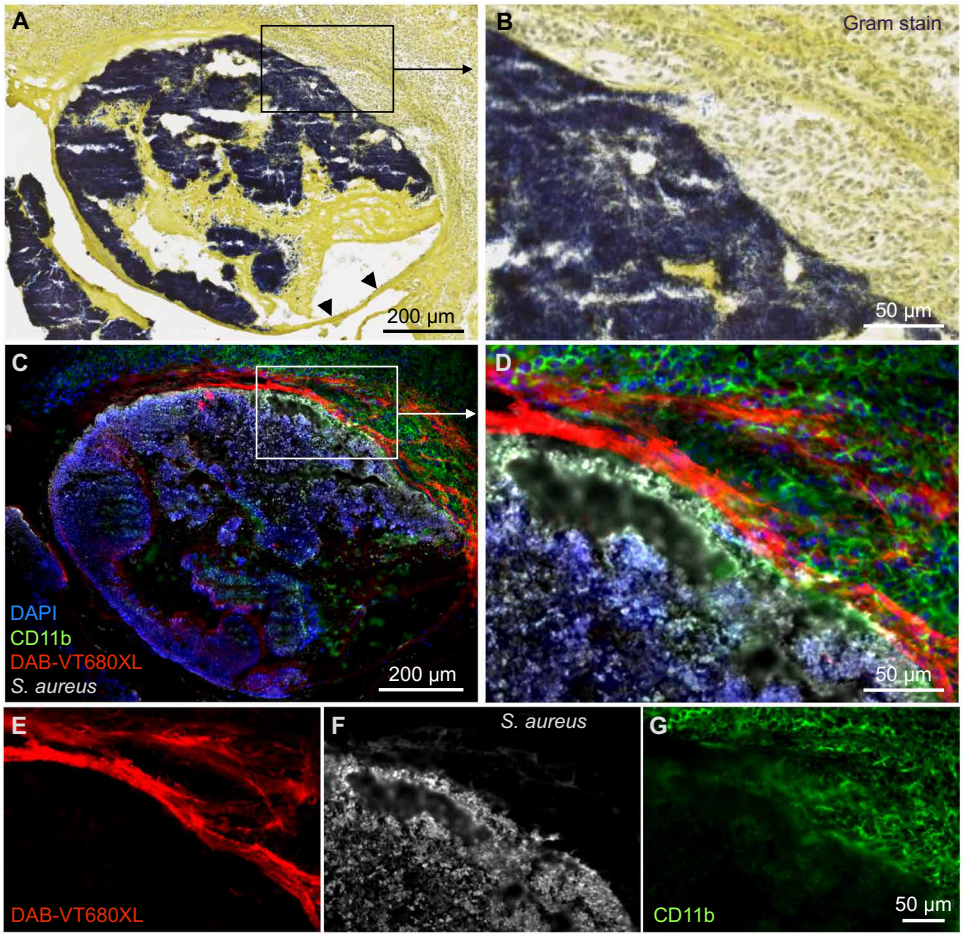

Fig. 3. DAB-VT680XL targeting of endocarditic vegetations in mice. (**A**) Gram stain of aortic root after inducing endocarditis in mice shows *S. aureus* in dark purple. Arrowheads indicate aortic valve leaflet. (**B**) High magnification view of boxed area in (A). (**C** and **D**) Adjacent sections of the endocarditic vegetation 90 min after DAB-VT680XL injection. DAPI, 4′,6-diamidino-2-phenylindole. DAB-VT680XL imaging signal (**E**) highlights the intersection of bacterial vegetations (**F**) with the host. Staining for CD11b (**G**) illustrates the distribution of myeloid cells, which are unable to enter the bacterial colony. The experiment was repeated twice with the same result.

DISCUSSION

Acute endocarditis, including heart valve infection caused by *S. aureus*, is difficult to manage, potentially deadly and on the rise (*1*, *2*, *10*). Here, we introduce imaging tools to monitor host *S. aureus* interactions and a strategy for adjuvant immunotherapy that neutralizes virulence factors and improves survival in mice.

Imaging agent codevelopment enables multimodal sensing of optical and radioisotope probes. We developed the PET agent ^{18}F-DAB because PET is the most sensitive and translatable molecular imaging modality, as demonstrated by its clinical track record (*11*–*13*). The limitations of PET imaging include relatively low spatial resolution and high costs. Codeveloping the fluorescent agent DAB-VT680XL with the same affinity ligand provides cellular resolution data for molecular targets imaged by PET. In conjunction with FMT, a quantitative imaging method available for noninvasive mouse studies, DAB-VT680XL proved useful in a preclinical neutralizing antibody trial in mice. A lower imaging signal in endocarditis vegetations echoed therapy-induced survival benefits, suggesting that this imaging biomarker may predict survival. We speculate that, in a clinical scenario, PET imaging with ^{18}F-DAB could track therapeutic efficiency in a trial of candidate drugs similar to the SC- and vWBp-neutralizing antibodies that we tested here in mice. If further development of this therapeutic strategy leads to a human trial and clinical use, then PET imaging with ^{18}F-DAB could identify patients in need of therapy or monitor therapeutic effects. The PET/MRI data in piglets with endocarditis indicate that combining molecular PET with MRI is particularly informative, as MRI provides outstanding soft tissue contrast and sufficient temporal and spatial information to visualize *S. aureus* vegetations. Given its capacity for bedside use, facile Doppler assessment of valve function, and lower cost, echocardiography will remain a mainstay for serially monitoring acute endocarditis. However, molecular PET/MRI, using either ^{18}F-DAB or other radioactive probes previously reported by others (*14*–*17*), has the potential to improve antibiotic selection and guide timing and extent of surgical interventions during key disease stages.

In contrast to other endocarditis imaging agents, ^{18}F-DAB and DAB-VT680XL do not directly bind bacteria but rather report on *S. aureus*' interaction with the host's clotting system, which contributes to biofilm formation (*9*). This fibrin-rich wall protects the bacterial colony against host immunity and—in combination with exopolysaccharides, extracellular DNA, and other factors—hinders penetration of antibiotics (*18*). Our data indicate that ^{18}F-DAB and DAB-VT680XL avidly bind to this critical vegetation component. Using DAB-VT680XL in intravital microscopy visualized innate immune cells' inability to penetrate the wall, swarm into the vegetation, and kill *S. aureus*. Treatment with antibodies against SC and vWBp decreased DAB-VT680XL uptake, and myeloid cells were able to enter the vegetations. Prior work has demonstrated a similar trend for DAB therapy in vitro (*19*, *20*); however, our microscopy data provide in vivo evidence of such host-pathogen interactions.

Noteworthy limitations related to the introduced PET/MRI approach include that the probe binds not only to vegetations but also to sterile thrombi. Clinically, differentiating between thrombus and vegetation can be difficult. Given this limitation, the presence of typical vegetation anatomy on MRI or clinical signs, as per the modified Duke criteria (*21*), may remain vital for interpreting PET signal. Another clinically relevant point that remains to be explored is prosthetic valve endocarditis, especially because metallic implants may cause MRI artifacts. Further, the imaging probe developed here targets specific host-pathogen interactions. Bacterial strains that do not enter those are outside the imaging probe's target range. Last,

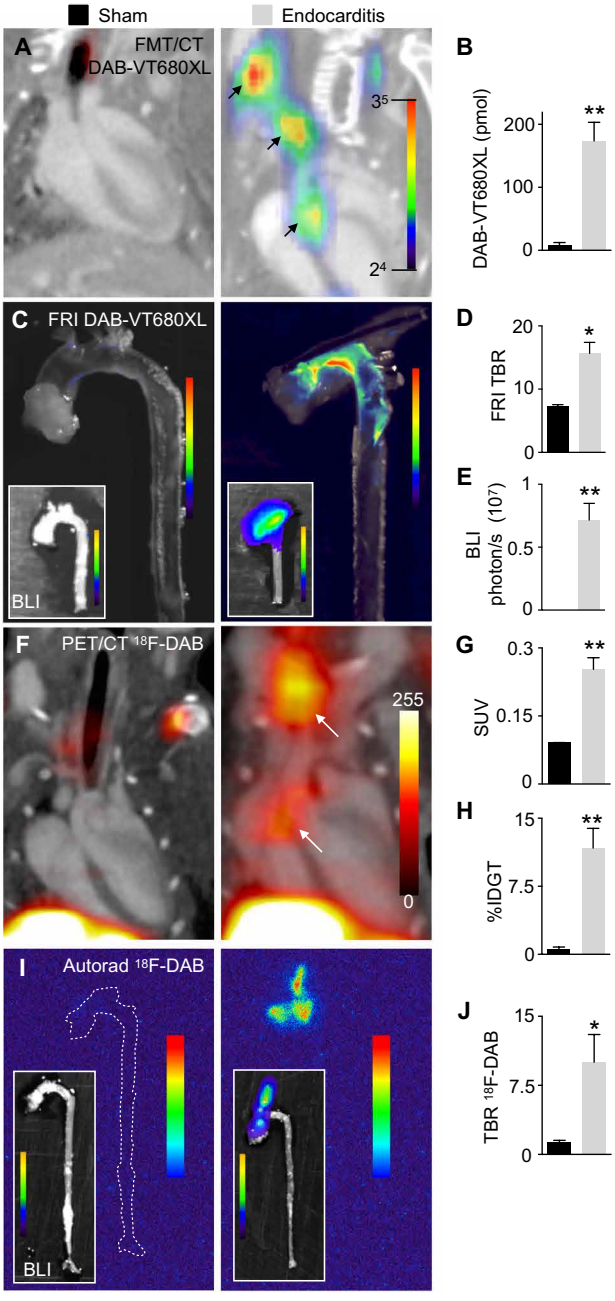

Fig. 4. Noninvasively imaging mouse endocarditis. (**A**) In vivo FMT/CT images and (**B**) fluorescence quantification in the aortic roots of mice with *S. aureus* endocarditis (right) and sham controls (left) ($n = 5$ to 8 mice per group; $P = 0.0055$). (**C**) Ex vivo fluorescence reflectance imaging (FRI) and bioluminescence imaging (BLI; insets) illustrate macroscopic colocalization of bacterial colonies with DAB-VT680XL imaging signal. (**D**) Quantification of fluorescence as target-to-background ratio (TBR) ($n = 5$ to 8 mice per group; $P = 0.0286$). (**E**) Quantification of BLI signal derived from bioluminescent *S. aureus* strain Xen29 ($n = 5$ to 8 mice per group; $P = 0.0095$). (**F**) PET/CT imaging after injection of ^{18}F-DAB. Arrows indicate signal from *S. aureus* vegetations on the aortic valves and the suture in the brachiocephalic artery. (**G**) In vivo quantification of PET signal in the aortic root (SUV; $n = 6$ to 10 mice per group, data from four separate experiments; $P = 0.0095$). (**H**) Ex vivo scintillation counting of aortic roots (%IDGT, percent injected dose per gram tissue; $n = 5$ to 12 mice per group; $P = 0.0052$). (**I**) Autoradiography of dissected aortas. Left: Sham-operated mouse with absent ^{18}F-DAB signal and absent bioluminescent signal indicating lack of bacteria. Right: With ^{18}F-DAB signal with colocalized bioluminescent bacterial colonies in the ascending aorta (inset). (**J**) Quantification of autoradiography (TBR; $n = 5$ to 7 mice per group, three separate experiments; $P = 0.037$). Unpaired, two-tailed *t* test was used, and data are shown as means ± SEM. $^*P < 0.05$ and $^{**}P < 0.01$.

the imaging target is specific to well-controlled, rare processes that occur in acutely forming clots and in the vegetation-host interface. The target abundance, as well as the resulting target-specific PET isotope concentration, is therefore lower than what is commonly obtained with imaging agents of broader specificity such as ^{18}F-fluorodeoxyglucose (^{18}F-FDG), warranting further optimization in large animals before first-in-human studies.

We chose to work with 3-week-old piglets because these smaller animals are easier to handle and less costly than adults. In general, swine disease models are considered similar to human pathologies and thus an attractive intermediate step for drug discovery and imaging agent development. Because it relies on two archetypical endocarditis triggers in humans, namely, a combination of an indwelling intravenous catheter or aortic valve damage with bacteremia, this animal model is particularly relevant to human disease. In addition to helping test therapeutics and imaging approaches in a human-like setting, the piglet model could be useful for research on surgical management, a potentially life-saving treatment that is still in need of optimization and standardization (*1*). Because pig hearts are similar to humans' in size and anatomy, experiments in pigs with endocarditis could address questions such as when and how to best replace an infected valve or remove vegetation and explore minimally invasive, catheter-based strategies.

S. aureus's coevolution with the human immune system endowed the bacteria with several efficient countermeasures against host defenses. These include bacterial factors that kill cells, inhibit the complement system, impede neutrophil and macrophage migration, evade phagocytosis, and facilitate bacterial survival after phagocytosis (*9*). Some virulence factors promote colonization of indwelling catheters by generating a biofilm. Typically, *S. aureus* endocarditis vegetations activate the host's clotting system to anchor the colony and surround it with a protective fibrin mesh. Upstream interventions that curtail bacterial virulence rather than host clotting factors could ultimately be a safer alternative. We detected decreased thrombin in mouse endocarditis vegetations after treatment with antibodies that neutralize SC and vWBp. In line with studies using knockout bacteria (*22*), we observed that vegetations still evolved and mice succumbed eventually; nevertheless, antibody treatment prolonged survival, whereas DAB-VT680XL signal decreased in the lesions and innate immune cells invaded bacterial colonies. Because of the differences between the mouse and human immune systems and prior failures to translate antibody therapeutics for *S. aureus* infections from mouse to man (*23*), it is unclear whether the introduced antibody neutralization of SC and vWBp will work in patients until this has been tested and whether such therapy is efficient if initiated during later disease stages. Thus, our data indicate that future work should investigate combining immunotherapy with antibiotics, a dual strategy that aims to augment the host's innate immunity and kill bacteria.

MATERIALS AND METHODS

Study design

The studies were designed to develop PET/MRI probes for bacterial endocarditis. Initial optical and nuclear imaging in mice was followed

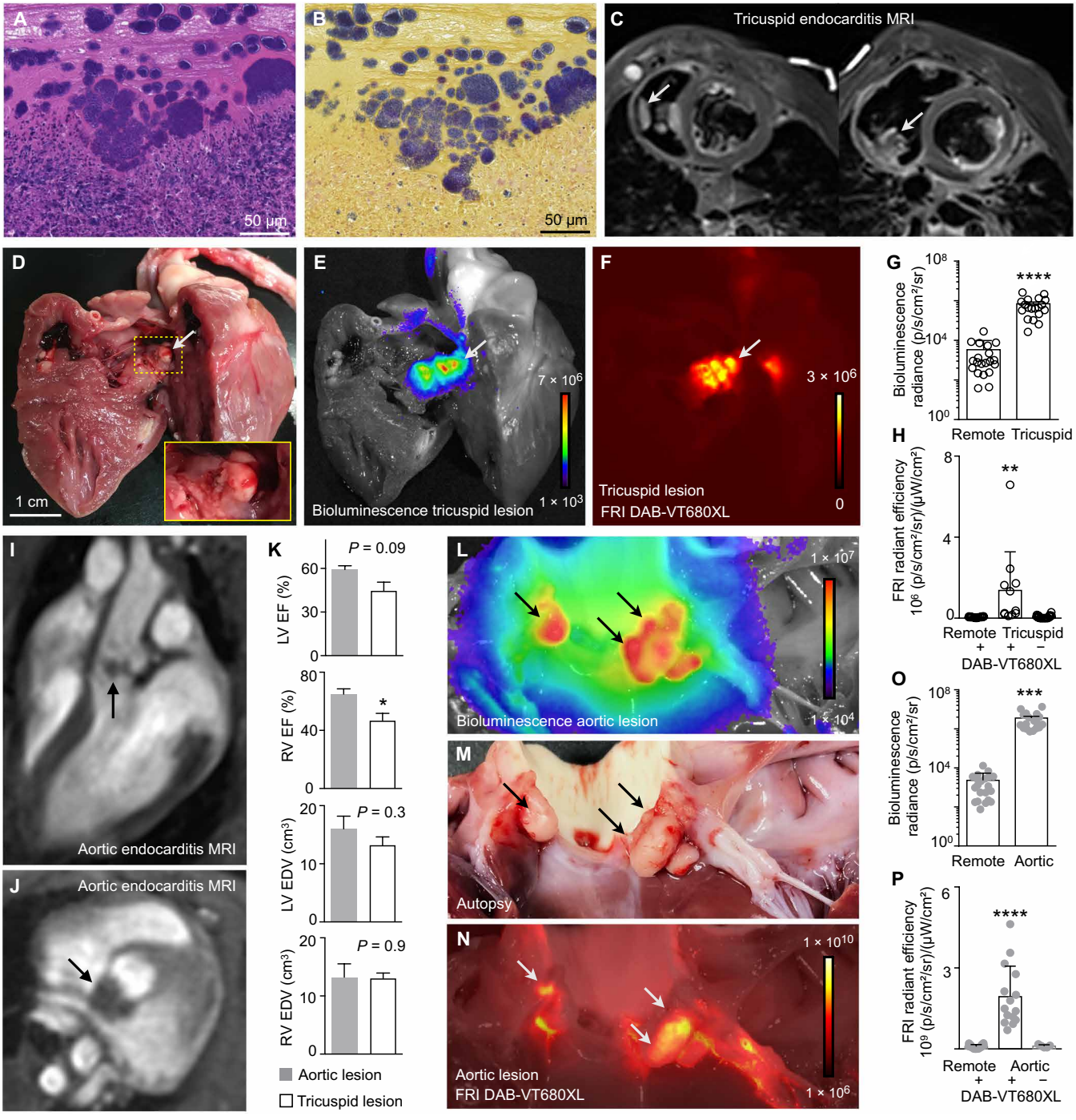

Fig. 5. *S. aureus* endocarditis in piglets. (**A**) H&E staining of right-sided piglet endocarditis vegetation indicating immune response to the *S. aureus* Xen36 infection. (**B**) Gram staining of an adjacent section showing the pathogen in the piglet heart. (**C**) Short-axis stacks of black blood MRI from a pig 10 days after induction of right-sided endocarditis. Arrows indicate vegetations. (**D**) View of the open right ventricle in piglet with right-sided endocarditis. Inset shows magnified view. (**E**) Bioluminescence image of (D) illustrates location of Xen36 *S. aureus*. (**F**) FRI of (D) and (E) indicates DAB-VT680XL imaging signal after intravenous injection of the near-infrared imaging agent. (**G**) Ex vivo quantification of bacterial bioluminescence from multiple vegetations of 12 piglets with right-sided endocarditis. Unpaired, two-tailed *t* test was used, and data are shown as means ± SEM, $^{****}P < 0.0001$. (**H**) FRI in a DAB-VT680XL–injected subset of piglet demonstrates accumulation of the imaging probe [$n = 3$ piglets per group, one-way analysis of variance (ANOVA) for multiple comparison, Barlett's test, $^{**}P < 0.01$]. (**I**) Long-axis and (**J**) short-axis MRI of piglet after induction of left-sided endocarditis. (**K**) Cardiac MRI–derived ejection fraction (EF) of the right and left ventricle (RV and LV, respectively) and the end-diastolic volumes (EDV), comparing left- with right-sided endocarditis ($n = 6$ piglets with tricuspid right-sided and $n = 4$ with aortic left-sided disease; two-tailed *t* test, $^{*}P < 0.05$). (**L**) BLI demonstrates bacterial infection, with signal arising from vegetations (arrows) identified on autopsy (**M**) and FRI (**N**). (**O**) Ex vivo quantification of bacterial bioluminescence in eight piglets with left-sided endocarditis; two-tailed *t* test., $^{***}P < 0.001$. (**P**) Quantification of fluorescence signal arising from aortic valve vegetations ($n = 5$ piglets; one-way ANOVA for multiple comparison with $^{****}P < 0.0001$, Barlett's test).

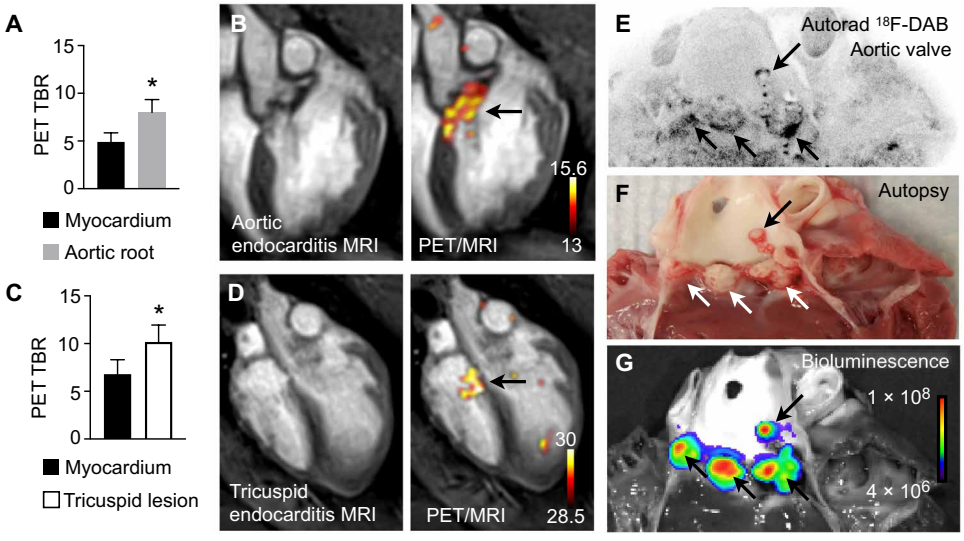

Fig. 6. PET/MRI *S. aureus* endocarditis in piglets. (**A**) Left-sided endocarditis TBR of PET signal, calculated with either myocardium (control) or vegetation-bearing aortic root as target and the skeletal muscle as background ($n = 3$ piglets; two-sided Student's t test, $^*P < 0.05$). (**B**) PET/MR images illustrating the imaging signal in aortic valve with endocarditis lesion (arrow). Color scale depicts becquerels per milliliter. (**C**) Right-sided endocarditis TBR, calculated as above ($n = 3$ piglets; two-sided Student's t test, $^*P < 0.05$). (**D**) PET/MR images illustrating the imaging signal in tricuspid valve endocarditis lesion (arrow). Color scale depicts becquerels per milliliter. (**E**) Ex vivo autoradiography of aortic valve indicates radioactive signal in the aortic valve vegetations, which were verified on autopsy (**F**) and a source of bioluminescence (**G**) arising from *S. aureus* (arrows).

by validation in a cohort of piglets subjected to either right- or left-sided endocarditis. The rationale was to improve imaging tools for monitoring host-pathogen interactions. Formal power estimations were not performed; however, the number of mice included per study ($n = 6$) was based on prior endocarditis imaging in mice (*7*). Mice were randomly assigned to disease and treatment groups. Investigators were not blinded to group allocation. Wherever possible, studies were repeated at least once. The number of animals used and experimental replicates performed are stated for each experiment in the figure legends.

Bacteria

Xen29 and Xen36 are both bioluminescent strains of coagulase-positive methicillin-susceptible *S. aureus*. Xen43 is *S. epidermidis* strain. All Xen strains were purchased from PerkinElmer Inc. *S. aureus*$^{RFP+}$ is a fluorescence version of methicillin-resistant *S. aureus* USA 300, NE1260R JE2 pckA::rfp that was obtained from J. Bose of University of Kansas Medical Center (*24*). Briefly, strains were cultured in liquid brain heart infusion broth under constant shaking at 150 to 200 rpm at 37°C. For injecting the animals, overnight cultures were diluted 20-fold in sterile Dulbecco's phosphate-buffered saline (PBS) without calcium or magnesium (Lonza). The injections' approximate CFU counts were assessed by light scattering at 600 nm using a Shimadzu UV-2101PC spectrophotometer according to the manufacturer's guidelines. Before injection, bioluminescence production was confirmed using a bioluminescence imager (LAS-1000, Fujifilm) set to 10-min integration time. After injection, true CFU numbers were verified by serial plating on 5% sheep blood agar (Hardy Diagnostics), and the expression of either the bioluminescent or fluorescent reporter gene was confirmed by imaging the agar plates. To maximize microbe pathogenicity for the porcine models, the Xen strain with strongest bioluminescence in the piglets was selected after a limited screen, and the porcine-passaged strain was cultured from a port abscess. All piglet experiments used this porcine-primed Xen36 strain.

Mouse endocarditis

To induce mouse endocarditis, we followed protocols for artery isolation surgery, 4.0 suture material insertion, and *S. aureus* infection as previously reported (*7*). A 4-0 suture was advanced through the surgically exposed right carotid artery into the left ventricular outflow tract and fixed in place. After a 24-hour recovery period, 1×10^6 CFU of *S. aureus* in 100 μl of PBS was injected through the tail vein. Continual endothelial damage to the aortic valve caused by the indwelling suture allowed the bacteria to attach and form vegetations. All animal experimentation and cohort size determination were approved in advance by the Massachusetts General Hospital's Subcommittee on Research Animal Care.

Mouse renal infection

Mice (n = 14 mice) were anesthetized with isoflurane (1 to 3%/2 liters of O_2) and received 6×10^7 CFU of *S. aureus* Xen36 in 50 μl of sterile PBS by intravenous injection. Mice were imaged for bioluminescence signal in the region of the kidneys starting at 48 hours after infection. Mice ($n = 8$) showing apparent kidney infection were separated, and half of those animals received the DAB-VT680XL (10 nmol) by intravenous injection. All mice were imaged at 24 hours after probe injection, when unbound DAB-VT680XL was excreted, and compared to noninfected control animals that only received the DAB-VT680XL injection (n = 3). Imaging entailed collection of both bioluminescence (300-s exposure time) and fluorescence (675-nm excitation and 720-nm emission filters) using an IVIS Lumina XRMS imaging system (PerkinElmer Inc.). Mice were euthanized, and confirmatory in situ and ex vivo images were also collected. All experimentation was approved by the Institutional Animal Care and Use Committee for Auburn University.

Piglet endocarditis

A total of 36 newly weaned piglets (16 to 20 days old, weighing 4.5 to 6.8 kg) were purchased from the Swine Research and Education Center at Auburn University for use in model development [bioluminescence imaging (BLI) only], fluorescence probe colocalization, and clinical PET/MRI studies. The animals were acclimated for 5 to 7 days before central-line implantation surgery. Piglets were sedated with dexmedetomidine (DEXDOMITOR, Zoetis) and butorphanol. An intravenous catheter was placed, and anesthesia was induced using a combination of ketamine (10 mg/kg; KETASET, Zoetis), dexmedetomidine (20 μg/kg), and butorphanol (0.4 mg/kg). A line block of 0.5% lidocaine (Xylocaine-MPF, Fresenius Kabi, USA) was placed before making a 3- to 4-cm incision just lateral to the midline. A combination of sharp and blunt dissection was used to identify and isolate the left jugular vein and then to create a subcutaneous pocket

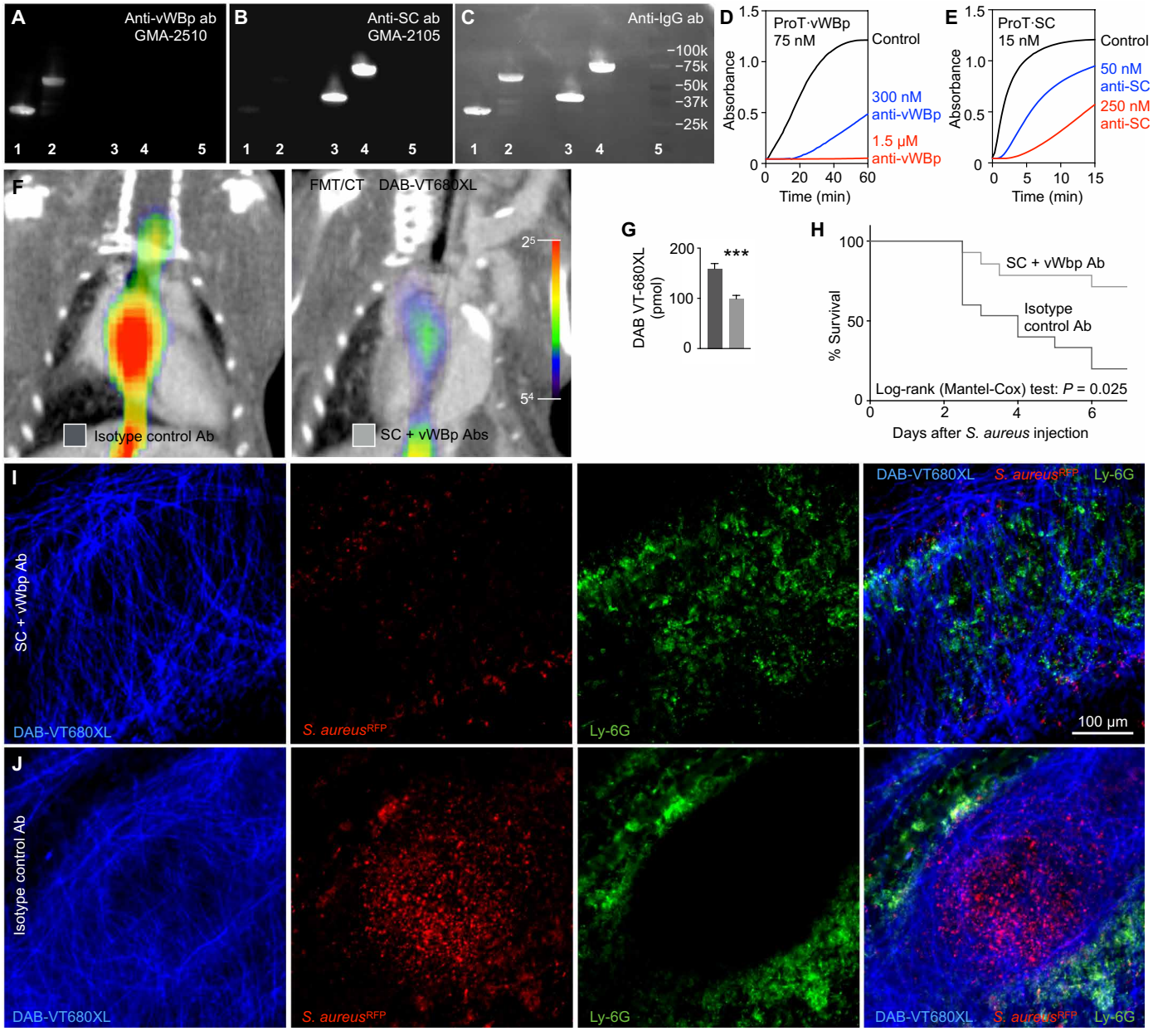

Fig. 7. Immunotherapy neutralizing virulence factors disrupts vegetations and improves survival. (**A** to **C**) Specificity of monoclonal antibodies by immunoblotting against vWBp-(1-263) in lane 1, vWBp-(1-474) in lane 2, SC-(1-325) in lane 3, and SC-(1-660) in lane 4. Lane 5 contains protein standards with the indicated molecular weights. The indicated antibodies, in (A) GMA-2510 monoclonal [anti–von Willebrand factor–binding protein (anti-vWBp)] and in (B) GMA-2105 monoclonal [anti-staphylocoagulase (anti-SC)], are specific for their respective targets. (C) shows probing for total mouse IgG (anti-IgG polyclonal against both the heavy and light chains of murine IgG) and reflects the bound antibodies shown in (A) and (B). (**D**) Increase in turbidity as measured by absorbance change at 450 nm for mixtures of fibrinogen (1.5 mg/ml) and 75 nM prothrombin complexed to vWBp-(1-263) (ProT·vWBp) complex in the absence of GMA-2510 antibody (anti-vWBp Ab; black line), in the presence of 300 nM anti-vWBp Ab (blue line) or 1.5 μM anti-vWBp Ab (red line). (**E**) Similar reactions for 15 nM prothrombin complexed to SC-(1-325) (ProT·SC) are shown in the absence of GMA-2105 antibody (anti-SC Ab; black line), in the presence of 50 nM anti-SC ab (blue line) or 250 nM anti-SC ab (red line). (**F**) In vivo FMT/CT images of *S. aureus* endocarditis in mice after injection of DAB-VT680XL treated with either isotype control antibody or antibodies neutralizing SC and vWBp. (**G**) In vivo fluorescence quantitation of vegetation thrombin in aortic roots after DAB-VT680XL injection ($n = 10$ to 12 mice per group, three separate experiments; unpaired, two-sided t test was used, and data are shown as means ± SEM; $^{***}P < 0.001$). (**H**) Kaplan-Meier survival curves of *S. aureus* endocarditis mice treated with isotype control antibody or combination therapy with anti-SC and anti-vWBp antibodies ($n = 15$ mice per group, mice received a single intraperitoneal injection of their respective antibody treatment 6 hours after surgery). (**I**) Intravital microscopy of femoral *S. aureus* vegetation 24 hours after intravenous injection of *S. aureus*$^{RFP+}$ and combination treatment with both anti-SC and anti-vWBp or (**J**) isotype control antibody. In vivo DAB-VT680 microscopy of the vegetation wall surrounding RFP^{+} bacteria and Ly-6G^{+} neutrophils.

for the vascular access port (VAP; 5 Fr ClearPort, Access Technologies). The vascular port consisted of a titanium outlet with a silicone septum and catheter. A small jugular venotomy was made, and a 0.6-mm guide wire was introduced into the vascular lumen. The polyurethane VAP catheter was placed over the guide wire and advanced into the right ventricle under fluoroscopic guidance. Correct positioning of the catheter was confirmed using multiple injections of radiopaque contrast under fluoroscopic observation. Ports were implanted in the front right region of the neck. Once the desired catheter positioning was confirmed, the VAP catheter was secured within the jugular vein with several circumferential sutures of 3-0 polypropylene (PROLENE, Ethicon). The catheter tubing was cut to an appropriate length and connected to the VAP that was then secured within the subcutaneous pocket with multiple polypropylene sutures. The surgical site was lavaged with saline and closed with 3-0 poliglecaprone 25 (MONOCRYL, Ethicon) in the subcutaneous and intradermal layers. A 22-gauge Posigrip Huber point needle was placed into the VAP, continued patency was confirmed, and the VAP was heparin-locked. The VAP site was marked with a permanent skin marker for ease of injection. The piglets then recovered from anesthesia. Analgesia was provided with carprofen (2.2 mg/kg per os every 12 hours; RIMADYL, Zoetis) and butorphanol (0.2 to 0.4 mg/kg, intramuscularly every 4 to 6 hours). At 6 to 8 hours after surgery, piglets were injected with 4×10^8 to 8×10^8 CFU of *S. aureus* Xen36 (PerkinElmer Inc.) through the VAP using a Huber needle. Thereafter, the port was flushed with 5 ml of sterile PBS.

For aortic valve endocarditis, piglets were similarly prepared, but the aorta was accessed via the left carotid artery. Aortic valve damage was induced by repeated passing of a 2.5-mm diameter cytology brush (Endoscopy Support Services) through the valve. The brush was positioned under fluoroscopy guidance aided by repeated contrast injection. A venous leg catheter was used to administer anesthesia and the *S. aureus* Xen36 inoculum (5×10^8 to 8×10^8 CFU), followed by a bolus 60-ml sterile saline flush.

For optical studies, piglets were injected with 0.4 μmol of DAB-VT680XL in 2 ml of sterile PBS via the ear vein using a 25-gauge butterfly. Animals were euthanized 10 to 12 hours later and, BLI and fluorescence reflectance imaging (FRI) were performed immediately after necropsy using an IVIS Lumina XRMS imaging system (PerkinElmer Inc.). For PET/MRI, piglets were transferred to Mt. Sinai Hospital. All experimentation and the transport were approved by the Institutional Animal Care and Use Committee for Auburn University under protocol no. 2016-2860.

Synthesizing fluorescent and fluorine-18–labeled DAB

The fluorescent and nuclear thrombin-specific imaging agents are derived from the FDA-approved thrombin inhibitor DAB. Synthesizing both agents requires converting the parent compound's carboxylic acid functionality to an amine, which can be further modified with either a fluorochrome or ^{18}F-prosthetic group.

Synthesizing DAB-NH_2

DAB (50 mg, 106 μmol) was suspended in dimethylformamide (DMF; 4.0 ml) in a 20-ml vial with a magnetic stir bar, to which *N*-Boc-2,2′-(ethylenedioxy)diethylamine (105 mg, 424 μmol) and 1-ethyl-3-(3-dimethylaminopropyl)carbodiimide (265 mg, 1.38 mmol) were then added. After stirring for 3 hours, the reaction mixture was concentrated to dryness, redissolved in dimethyl sulfoxide:H_2O (2.0:0.1 ml), and subjected to reversed-phase chromatography, resulting in 50 mg for a 67.2% isolated yield of DAB-NH-Boc. LC–electrospray ionization (ESI)–MS(+) mass/charge ratio (m/z) = 702.5 $[M + H^+]^+$. DAB-NH-Boc was dissolved in H_2O:MeCN (1:1, 400 μl), and then HCl (4 M) in dioxane (1 ml) was added. The homogeneous solution was stirred at room temperature (RT) for 30 min, and the reaction was concentrated by rotovap to give 41 mg, a 95.6% yield, of DAB-NH_2 as a colorless solid. LC-ESI-MS(+) m/z = 602.4 $[M + H^+]^+$; LC-ESI-MS(−) m/z = 600.4 $[M - H^+]^-$.

Synthesizing DAB-VT680XL

DAB-NH_2 (0.5 mg, 0.7 μmol) was dissolved in DMF (12 μl) in a 1.5-ml centrifuge tube and added to VT680XL–*N*-hydroxysuccinimide (NHS) ester (1.0 mg, 0.7 μmol) in DMF (100 μl). After 3 hours, this mixture was concentrated to dryness then redissolved in H_2O/MeCN (10:1, 110 μl) and subjected to C18 reverse-phase high-performance LC (HPLC) purification. The combined HPLC collections were concentrated to give 1.1 mg of product, a 75.6% yield. LC-ESI-MS(−) m/z = 917.4 $([M - 2H^+]/2)^-$ and 611.2 $([M - 3H^+]/3^-$.

Synthesizing ^{19}F-DAB

DAB-NH_2 (4 mg, 6.7 μmol) was dissolved in DMF (100 μl) and triethylamine (3 μl) in a 1.5-ml centrifuge tube and treated with *N*-succinimidyl-4-fluorobenoate (3 mg, 12.5 μmol) in DMF (50 μl). After 4 hours, the mixture was concentrated by rotary evaporation and subjected to HPLC purification resulting in 4.1 mg of ^{19}F-DAB, a 68% yield. LC-ESI-MS(+) m/z = 724.6 $[M + H^+]^+$ and 746.6 $[M + Na^+]^+$.

Synthesizing ^{18}F-DAB

The prosthetic group *N*-succinimidyl-4-[^{18}F]-fluorobenzoate (^{18}F-SFB) was synthesized after the automated procedure of Scott and Shao (*25*), adapted for a Synthra RNplus automated synthesizer (Synthra GmbH) operated by SynthraView software. Starting with [^{18}F]-F-, no-carrier-added, [~1772 megabecquerels (MBq), 50 ± 4 mCi], ^{18}F-SFB was prepared in 25.0% isolated yield in 100 min. DAB-NH_2 (4 mg, 6.7 μmol) dissolved in acetonitrile (500 μl), and triethylamine (4 μl) was reacted with ^{18}F-SFB (447 MBq, 12 ± 3 mCi) at 65°C for 5 min, cooled and subjected to C18 reverse-phase HPLC using a MACHEREY-NAGEL NUCLEODUR C18 Pyramid 250 × 10 mm VarioPrep column eluted with 75:25 water/acetonitrile (100 mM ammonium formate) at 5.5 ml/min and a 254-nm ultraviolet (UV) detector and radiodetector connected in series. ^{18}F-DAB was synthesized in 10.7% isolated yield (189 MBq, 5.1 ± 0.2 mCi) and at 99 ± 0.9% radiochemical purity.

^{18}F-DAB for piglet imaging was produced using a GE FX2N automated synthesizer (GE Healthcare). A quaternary methyl ammonium cartridge containing cyclotron-produced [^{18}F]fluoride (~30 GBq, 0.81 ± 0.05 Ci) was eluted with a solution containing 9 mg of 4,7,13,16,21,24-hexaoxa-1,10 diazabicyclo[8.8.8]hexacosane (Kryptofix 2.2.2), 0.08 ml of 0.15 M K_2CO_3, and 1.92 ml of acetonitrile into a 5-ml reaction vial. Solvents were removed azeotropically at 110°C under a slight flow of helium. Then, ^{18}F-SFB was synthesized in 30% isolated yield (as described in the previous section) and reacted with DAB-NH_2 (4 mg, 6.7 μmol) dissolved in acetonitrile (500 μl) and triethylamine (4 μl) at 65°C for 5 min. The reaction mixture was purified by HPLC using a C18 semipreparative column (250 × 10 mm, 5 μm; Luna C18, Phenomenex) and isocratic elution with 90:10 water (75 mM ammonium formate)/ethanol at 5 ml/min and a 254-nm UV detector. ^{18}F-DAB was synthesized in 8 ± 1.2% decay-corrected radiochemical yield (2.3 ± 1.1 GBq, 0.06 ± 0.03 Ci, at RT for 32 min) and at >98% radiochemical purity. Purity was assessed

via Radio-HPLC using a C18 analytical column (100 Å, 250 × 4.6 mm, 5 μm, at RT for 9.8 min; Atlantis T3, Waters, Milford, MA, USA).

Thrombin activity assay

To confirm that modification did not inhibit binding activity, VT680XL and ^{19}F labeled DAB were examined with the SensoLyte AFC Thrombin Assay Kit (AnaSpec). Thrombin cleaves the substrate, releasing 7-amido-4-trifluoromethylcoumarin, which was monitored at an excitation/emission of 380/500 nm.

^{18}F-DAB blood half-life

To determine the blood half-life of the ^{18}F-labeled imaging agent derived from the thrombin inhibitor DAB (^{18}F-DAB), the blood from ^{18}F-DAB–injected mice was collected by retro-orbital bleeding and sampled with gamma counter. Under isoflurane (1.5 to 3%) anesthesia, ^{18}F-DAB was injected via tail vein (about 250 μCi in 100 μl of PBS) in six 12-week-old C57BL/6 mice. Mice were kept on a heated stage (37°C) under isoflurane anesthesia and bled 20 μl 1 to 2, 5, 10, 15, 30, 60 and 120 min after probe injection. Blood samples were weighed, and residual radioactivity in the samples was measured using a gamma counter and the percent injected dose per gram blood (%IDGB) was computed. Blood half-life was derived from fitting %IDGB to the one compartment pharmacokinetic equation $C(t) = C(o)e^{-kt}$, where $C(t)$ is %IDGB at time t and k is the rate constant. Half-life is denoted as $t_{1/2} = \frac{ln(2)}{k}$.

Intravital microscopy of thrombi in the femoral artery

We used intravital microscopy to visualize DAB-VT680XL binding to freshly formed thrombi. Arterial thrombosis was induced by applying ferric chloride solution (500 mM concentration; Sigma-Aldrich) on the exposed femoral artery of mice. Fluorescently conjugated anti-CD41 monoclonal antibody (mAb) (BioLegend) was injected via tail vein to label platelets in vivo before thrombosis induction. DAB-VT680XL and control fluorochrome VT680XL were injected intravenously 5 min after thrombosis induction. Images were acquired with in vivo microscopy (Olympus).

Intravital microscopy of vegetation in the femoral artery

A 12-0 Ethicon suture material was inserted into the saphenous artery, advanced into the femoral artery, and fixed in position while maintaining sufficient blood flow. Mice were allowed to recover for 6 hours before injection of 10^6 CFU of *S. aureus*$^{RFP+}$ bacteria in 100 μl of PBS. Six hours after bacteria administration, SC- and vWBp-neutralizing mAb (GMA-2105 and GMA-2510, Green Mountain Antibodies) or isotype immunoglobulin G (IgG)–control antibodies were injected. Ninety minutes before imaging, neutrophils were labeled by injecting 15 μg of fluorescein isothiocyanate (FITC) anti-mouse Ly-6G antibody (clone 1A8, BioLegend), and the vegetation was stained by injecting 2 nmol of DAB-VT680XL. All injections were performed via tail vein. Intravital microscopy was performed 24 hours after bacteria injection. Mice were anesthetized using 1 to 2% isoflurane and then placed on a heated (37°C) stage for imaging, and the wound was reopened. Imaging was performed using an Olympus (IV100) microscope with a water-immersion objective (UMPlanFL N 20×/0.50 numerical aperture, Olympus). Three channels were recorded (Ly-6G FITC, 488-nm excitation; RFP, 561-nm excitation; DAB-VT680XL, 647-nm excitation) to generate *z*-stacks at 2-μm steps. Image postprocessing was performed using ImageJ software.

Fluorescence molecular tomography/x-ray computed tomography

On day 3 after suture insertion and 48 hours after injection of either 1×10^6 CFU of *S. aureus* Xen29 in 100 μl of PBS or PBS only for the sham group, FMT/CT imaging was performed. To this end, mice were injected with 2 nmol of the fluorescent imaging probe and imaged 2 hours later using the FMT 2500 LX Quantitative Tomography Imaging System (PerkinElmer Inc.). After excitation at 680 nm and emission collection at 700 nm, a three-dimensional dataset containing fluorescence concentration per voxel was reconstructed. FMT imaging was accompanied by hybrid x-ray CT angiography (Inveon PET/CT, Siemens). Image fusion was achieved using OsiriX software and fiducial markers on a dedicated multimodal imaging cassette frame, as described previously (*26*). During CT acquisition, ISOVUE 370 was infused at 50 μl/min through a tail vein catheter. The CT was reconstructed using a modified Feldkamp cone-beam reconstruction algorithm (COBRA, Exxim Inc.), bilinear interpolation, and a Shepp-Logan reconstruction filter. Voxels were scaled to Hounsfield units. The isotropic spatial resolution was 110 μm for CT and 1 mm for FMT. Fused datasets were used to place regions of interest (ROIs) in the left ventricular outflow tract and the aortic valve region. After FMT/CT, underwent ex vivo fluorescence imaging of excised aortas on an OV-110 epifluorescence microscope (Olympus). The same setup was used to evaluate the effects of SC- and vWBp-neutralizing mAb treatment. Six hours after bacteria injection, either SC- and vWBp-neutralizing mAb or unspecific IgG control antibodies were injected.

FRI and histology

Excised aortas were imaged side by side with controls using epifluorescence microscope (OV-110, Olympus). The tissue was then fixed in 4% paraformaldehyde for at least 12 hours, embedded in optimal cutting temperature compound, and flash-frozen in an isopentane/dry ice bath. H&E, Gram staining (Sigma-Aldrich), and immmunofluorescence staining for CD11b were performed to verify the presence of *S. aureus* bacteria and myeloid cells on the aortic valve. Fluorescence microscopy (Eclipse 80i, Nikon) was performed to investigate microscopic DAB-VT680XL localization in the vegetation, and bright-field images were scanned and analyzed using a Nanozoomer 2.0RS (Hamamatsu).

PET/CT imaging in mice

On day 3 after surgery, animals were injected with 250 μCi of ^{18}F-DAB and imaged by PET-CT 1.5 hours later. We used an Inveon small-animal PET-CT scanner (Siemens), a three-dimensional ordered subsets maximum likelihood with maximum a posteriori (OSEM3D/MAP) algorithm with 2 OSEM and 18 MAP iterations to reconstruct into three-dimensional images. The CT was performed before the PET scan. The PET voxel size was 0.796 mm by 0.861 mm by 0.861 mm, for a total of 128 voxel by 128 voxel by 159 voxel. Standard uptake values (SUVs) were obtained from manually drawn ROIs in the invent research workplace software environment. After PET/CT imaging, the aortic root was excised, counted on a Wallac wizard 3 gamma counter to obtain percent injected dose per gram tissue (%IDGT) and imaged for bioluminescent signal. This was followed by overnight exposure on an autoradiography cassette. Plates were read on the Typhoon 9400 Variable Mode Imager (GE Healthcare). Target to background of both the bioluminescent signal and autoradiography was quantified using manual ROIs of the aorta and background in Amira software (Thermo Fisher Scientific).

Generating monoclonal antibodies that neutralize SC and vWBp

The murine monoclonal antibodies against synthetic peptides corresponded to the N-terminal residues 1 to 10 of either SC or vWBp from *S. aureus* Newman D2 Tager 104 strain (*27*). Corresponding peptides were synthesized with an additional C-terminal cysteine that conjugated to keyhole limpet hemocyanin (KLH) and ovalbumin (OA) using *m*-maleimidobenzoyl–NHS ester (*28*). To generate these monoclonal antibodies, mice were injected on day 1 with KLH-peptide conjugate (100 μg) in complete Freund's adjuvant. On days 17, 27, and 42, mice were injected with KLH-peptide conjugate (50 μg) in incomplete Freund's adjuvant. Serum titers from each mouse were determined by solid-phase enzyme-linked immunosorbent assay (ELISA), and spleen cells from the mouse with the highest serum titer were fused to NS1 myeloma cells on day 162, as described using polyethylene glycol (PEG) (*29*, *30*). Hybridoma was selected using hypoxanthine, azaserine, and thymidine. Fusion clones were screened by solid-phase ELISA with peptide-OA–coated microtiter plates. Selected clones showing signal above ~2× background were expanded, rescreened, subcloned three times by limiting dilution and stored in liquid nitrogen. SC-specific antibodies were designated GMA-2105, and others specific for vWBp were designated GMA-2510. Hybridoma cells were grown in Hybridoma-SFM media (Gibco) and antibodies purified by protein G affinity chromatography. Purified antibody was sterile-filtered and stored at 4°C. Antibody aggregation was ruled out by size exclusion chromatography on an S-300 column and dynamic light scattering with a Zetasizer Nano S instrument (Malvern Panalytical). The isotype of each respective antibody was independently verified using/via goat anti-mouse isotype-specific antibody (Bethyl Laboratories) using a MAGPIX (Luminex).

Antibody specificity for SC and vWBp

Western blot confirmed specificity of prothrombin activation–specific monoclonal antibodies. Previously characterized recombinant proteins (*5*, *31*) were subjected to SDS–polyacrylamide gel electrophoresis with lanes corresponding to (i) vWBp-(1-263), (ii) vWBp-(1-474), (iii) SC-(1-325), (iv) SC-(1-660), and (v) protein standards with indicated molecular weights. The elaborated proteins were transferred to polyvinylidene difluoride membrane for Western blot analysis to probe the specificity and cross-reactivity of the monoclonal antibodies targeting the critical N termini of either SC or vWBp. The same blot was probed with either the anti-vWBp monoclonal antibody (GMA-2510) (5 μg/ml) or the anti-SC (GMA-2105) (10 μg/ml) for 1 hour at 4°C. After primary antibody treatment, blots were washed and probed with horseradish peroxidase–labeled rabbit anti-mouse IgG that lacked the constant region and then imaged for chemiluminescence substrate oxidation using a Fujifilm LAS-1000. The blot was stripped between primary antibody challenges. Last, because the antibodies were intended to be used together, we verified that GMA-2510 and GMA-2105 would have additive functions in recognizing these *S. aureus* virulence factors. To accomplish this, the blot was probed with the both the SC and vWBp neutralizing antibodies and then stained for total mouse IgG content using an anti-mouse IgG (H + L)–FITC polyclonal antibody. The blot was imaged for fluorescence using a Fujifilm FLA-5100 with the 473-nm laser and the long pass blue channel.

Fibrinogen turbidity assays

Cleavage of fibrinogen by either prothrombin·vWBp-(1-263) or prothrombin·SC-(1-325) complexes was monitored from the increase in turbidity at 450 nm at 25°C in 50 mM Hepes, 110 mM NaCl, 5 mM $CaCl_2$, PEG 8000 (1 mg/ml) (pH 7.4) buffer using the SpectraMax 340PC384 plate reader (Molecular Devices Inc.). Individual reaction conditions were tested to determine the effect of the respective antibodies on the ability of either vWBp or SC to activate prothrombin and subsequently cleave of fibrinogen. GMA-2510 (anti-vWBp Ab) was incubated with vWBp-(1-263), and GMA-2105 (anti-SC Ab) was incubated with SC-(1-325) for 25 min at 25°C before addition of prothrombin. The three components were then incubated together for an additional 25 min at 25°C prior subsampling into the turbidity assay. The vWBp assays had final concentrations of 75 nM prothrombin·vWBp-(1-263) complex with 0 nM, 300 nM, or 1.5 μM anti-vWBp Ab. The SC assays had 15 nM prothrombin·SC-(1-325) complex with 0, 50, or 300 nM anti-SC Ab. Fibrinogen (1.5 mg/ml) was added simultaneously to initiate all reactions. Progress curves were collected over time ranges necessary to observe total substrate depletion under the positive control conditions.

Survival study

To determine the potentially beneficial impact of eliminating prothrombin activation by bacteria, we simultaneously administered either both GMA-2105 and GMA-2510 mAbs or an isotype control mAb (Green Mountain Antibodies, Burlington, VT). Endocarditis was induced in 30 mice, which were randomized to treatment groups. Six hours after surgery, the mice received GMA-2105, GMA-2510, or isotype-labeled mAbs by intraperitoneal injection. Mice were kept under normal husbandry without further treatment except for pain management with buprenorphine as needed until death occurred, and humane end points were reached or up to day 7 after injection of 1×10^6 CFU of *S. aureus*.

MRI of piglets

Left ventricular ejection fraction was quantified from retrospectively gated short-axis cardiac cine MR images (Siemens 3T Biograph mMR). Acquisition parameters for cine short-axis stacks were as follows: a repetition time (TR) of 56.24 ms, an echo time (TE) of 3.32 ms, a number of averages of 2, 24, or 30 slices, 25 cardiac frames, 3-mm slice thickness, no interslice gap, a flip angle of 12, and a spatial resolution of 0.94 mm by 0.94 mm. Retrospective electrocardiogram (ECG) gating was used to acquire the images. ROIs were manually segmented with OsiriX MD v 9.5.1 and exported using the "Export ROIs" OsiriX plugin. The cine acquisition contains a total of 600 or 750 images from 24 slices with 25 cardiac frames per slice. Right ventricle vegetations were quantified from an ECG-triggered axial T2-weighted turbo spin echo (TSE) stack using the after acquisition parameters: a TR of 1125 to 1485 ms, a TE of 76 ms, a number of averages of 4 and 11 to 24 slices, 3-mm slice thickness, no interslice gap, a spatial resolution of 0.94 mm by 0.94 mm. ROIs were manually segmented with OsiriX MD v 9.5.1. ROIs were exported using the Export ROIs OsiriX plugin. Vegetations were segmented as high intensity areas within the right ventricle while excluding the catheter whenever possible.

PET/MRI of piglets

Eight piglets underwent imaging with a clinical PET/MR system (Siemens 3T Biograph mMR). The piglets received an intravenous injection of ^{18}F-DAB (51.8 and 25 MBq, respectively) 90 min before PET acquisition. Piglets were intubated and placed on the scanner bed under isoflurane anesthesia at 1.5 to 2% by inhalation and were

oxygenated throughout the PET/MRI experiment. Vital parameters were monitored. A six-channel body matrix product coil was used for signal reception. After scout scans, a static thoracic PET was performed for 60 min while simultaneously acquiring cardiac and T2-weighted TSE anatomical MR images as detailed above. Attenuation correction of PET images was performed using a vendor built-in Dixon MR-based attenuation map (MR-AC) with four tissue compartments (soft tissue, fat, lung, and air). Images were reconstructed using a three-dimensional ordinary Poisson ordered subset expectation maximization (OP-OSEM) algorithm with point spread function resolution modeling, using 3 iterations and 21 subsets and filtered with a 4-mm Gaussian filter.

Autoradiography of piglet samples

After euthanasia, animals were perfused, and heart samples were excised. To determine radiotracer distribution, digital autoradiography was performed by placing tissue samples in a film cassette against a phosphorimaging plate (BASMS-2325, Fujifilm) for 12.5 hours at −20°C. Phosphorimaging plates were read at a pixel resolution of 25 μm with a Typhoon 7000IP plate reader (GE Healthcare). Quantification was carried out using ImageJ software.

Statistical analysis

Results are reported as means ± SEM. Statistical analysis was performed using GraphPad Prism 7 software (GraphPad Software Inc.). Normal distribution of variables was tested using the Kolmogorov-Smirnov test or the D'Agostino-Pearson omnibus normality test. Data were analyzed by parametric tests if normal distribution was detected. An unpaired Student's t test was applied for two-group comparisons, and data were presented as means ± SEM with significance indicated by $^{*}P < 0.05$, $^{**}P < 0.01$, $^{***}P < 0.001$, and $^{****}P < 0.001$. If more than two groups were compared, then one-way analysis of variance (ANOVA) analysis and Bartlett's test for equal variances was used. If data were nonnormally distributed, then differences were evaluated using an unpaired, nonparametric Mann-Whitney test. A log-rank test was applied in the survival study. Significance level in all tests was 0.05. Raw data are provided in data file S1.

SUPPLEMENTARY MATERIALS

stm.sciencemag.org/cgi/content/full/12/568/eaay2104/DC1

Fig. S1. Blocking experiment indicates specificity of DAB-VT680XL.

Fig. S2. DAB-VT680XL does not enrich in acute myocardial infarcts.

Fig. S3: FMT in mice with endocarditis induced by *S. epidermidis* Xen43.

Fig. S4. Fluorescence imaging of renal *S. aureus* infection with DAB-VT680XL.

Fig. S5. DAB-VT680XL correlates with bacterial bioluminescence.

Movie S1. Midventricular short-axis cine MRI covering the cardiac cycle in a piglet with endocarditis.

Movie S2. Stack of short-axis views covering the heart of a piglet with endocarditis.

Movie S3. Intravital microscopy of *S. aureus* vegetation in the femoral artery of a live mouse treated with isotype control antibody.

Movie S4. Intravital microscopy of *S. aureus* vegetation in the femoral artery of a mouse.

Data file S1. Raw data.

View/request a protocol for this paper from *Bio-protocol*.

REFERENCES AND NOTES

1. S. Y. Tong, J. S. Davis, E. Eichenberger, T. L. Holland, V. G. Fowler Jr., *Staphylococcus aureus* infections: Epidemiology, pathophysiology, clinical manifestations, and management. *Clin. Microbiol. Rev.* **28**, 603–661 (2015).
2. T. J. Cahill, L. M. Baddour, G. Habib, B. Hoen, E. Salaun, G. B. Pettersson, H. J. Schäfers, B. D. Prendergast, Challenges in infective endocarditis. *J. Am. Coll. Cardiol.* **69**, 325–344 (2017).
3. L. Loeb, The influence of certain bacteria on the coagulation of the blood. *J. Med. Res.* **10**, 407–419 (1903).
4. R. Friedrich, P. Panizzi, P. Fuentes-Prior, K. Richter, I. Verhamme, P. J. Anderson, S. Kawabata, R. Huber, W. Bode, P. E. Bock, Staphylocoagulase is a prototype for the mechanism of cofactor-induced zymogen activation. *Nature* **425**, 535–539 (2003).
5. H. K. Kroh, P. Panizzi, P. E. Bock, Von Willebrand factor-binding protein is a hysteretic conformational activator of prothrombin. *Proc. Natl. Acad. Sci. U.S.A.* **106**, 7786–7791 (2009).
6. P. Panizzi, R. Friedrich, P. Fuentes-Prior, K. Richter, P. E. Bock, W. Bode, Fibrinogen substrate recognition by staphylocoagulase.(pro)thrombin complexes. *J. Biol. Chem.* **281**, 1179–1187 (2006).
7. P. Panizzi, M. Nahrendorf, J. L. Figueiredo, J. Panizzi, B. Marinelli, Y. Iwamoto, E. Keliher, A. A. Maddur, P. Waterman, H. K. Kroh, F. Leuschner, E. Aikawa, F. K. Swirski, M. J. Pittet, T. M. Hackeng, P. Fuentes-Prior, O. Schneewind, P. E. Bock, R. Weissleder, In vivo detection of *Staphylococcus aureus* endocarditis by targeting pathogen-specific prothrombin activation. *Nat. Med.* **17**, 1142–1146 (2011).
8. M. Peetermans, L. Liesenborghs, K. Peerlinck, E. V. Wijngaerden, O. Gheysens, K. E. Goffin, M. F. Hoylaerts, M. Jacquemin, J. Verhaegen, W. E. Peeterman, P. Verhamme, T. Vanassche; Staphylothrombin Investigators, Targeting coagulase activity in *Staphylococcus aureus* bacteraemia: A randomized controlled single-centre trial of staphylothrombin inhibition. *Thromb. Haemost.* **118**, 818–829 (2018).
9. T. J. Foster, Immune evasion by staphylococci. *Nat. Rev. Microbiol.* **3**, 948–958 (2005).
10. P. Panizzi, J. R. Stone, M. Nahrendorf, Endocarditis and molecular imaging. *J. Nucl. Cardiol.* **21**, 486–495 (2014).
11. A. J. Sinusas, F. Bengel, M. Nahrendorf, F. H. Epstein, J. C. Wu, F. S. Villanueva, Z. A. Fayad, R. J. Gropler, Multimodality cardiovascular molecular imaging, part I. *Circ. Cardiovasc. Imaging* **1**, 244–256 (2008).
12. R. Weissleder, M. Nahrendorf, Advancing biomedical imaging. *Proc. Natl. Acad. Sci. U.S.A.* **112**, 14424–14428 (2015).
13. M. Schwaiger, K. Kunze, C. Rischpler, S. G. Nekolla, PET/MR: Yet another Tesla? *J. Nucl. Cardiol.* **24**, 1019–1031 (2017).
14. X. Ning, S. Lee, Z. Wang, D. Kim, B. Stubblefield, E. Gilbert, N. Murthy, Maltodextrin-based imaging probes detect bacteria in vivo with high sensitivity and specificity. *Nat. Mater.* **10**, 602–607 (2011).
15. F. J. Hernandez, L. Huang, M. E. Olson, K. M. Powers, K. M. Hernandez, D. K. Meyerholz, D. R. Thedens, M. A. Behlke, A. R. Horswill, J. O. McNamara II, Noninvasive imaging of *Staphylococcus aureus* infections with a nuclease-activated probe. *Nat. Med.* **20**, 301–306 (2014).
16. K. L. Pinkston, K. V. Singh, P. Gao, N. Wilganowski, H. Robinson, S. Ghosh, A. Azhdarinia, E. M. Sevick-Muraca, B. E. Murray, B. R. Harvey, Targeting pili in enterococcal pathogenesis. *Infect. Immun.* **82**, 1540–1547 (2014).
17. C. T. Yang, K. K. Ghosh, P. Padmanabhan, O. Langer, J. Liu, D. Eng, C. Halldin, B. Gulyás, PET-MR and SPECT-MR multimodality probes: Development and challenges. *Theranostics* **8**, 6210–6232 (2018).
18. S. Periasamy, H. S. Joo, A. C. Duong, T. H. Bach, V. Y. Tan, S. S. Chatterjee, G. Y. Cheung, M. Otto, How *Staphylococcus aureus* biofilms develop their characteristic structure. *Proc. Natl. Acad. Sci. U.S.A.* **109**, 1281–1286 (2012).
19. T. Vanassche, J. Verhaegen, W. E. Peetermans, M. F. Hoylaerts, P. Verhamme, Dabigatran inhibits *Staphylococcus aureus* coagulase activity. *J. Clin. Microbiol.* **48**, 4248–4250 (2010).
20. T. Vanassche, J. Verhaegen, W. E. Peetermans, J. V. A. N. Ryn, A. Cheng, A. Schneewind, M. F. Hoylaerts, P. Verhamme, Inhibition of staphylothrombin by dabigatran reduces *Staphylococcus aureus* virulence. *J. Thromb. Haemost.* **9**, 2436–2446 (2011).
21. P. E. Fournier, J. P. Casalta, G. Habib, T. Messana, D. Raoult, Modification of the diagnostic criteria proposed by the Duke Endocarditis Service to permit improved diagnosis of Q fever endocarditis. *Am. J. Med.* **100**, 629–633 (1996).
22. S. Mancini, F. Oechslin, C. Menzi, Y. A. Que, J. Claes, R. Heying, T. R. Veloso, T. Vanassche, D. Missiakas, O. Schneewind, P. Moreillon, J. M. Entenza, Marginal role of von Willebrand factor-binding protein and coagulase in the initiation of endocarditis in rats with catheter-induced aortic vegetations. *Virulence* **9**, 1615–1624 (2018).
23. V. G. Fowler, R. A. Proctor, Where does a *Staphylococcus aureus* vaccine stand? *Clin. Microbiol. Infect.* **20**, 66–75 (2014).
24. J. L. Bose, P. D. Fey, K. W. Bayles, Genetic tools to enhance the study of gene function and regulation in *Staphylococcus aureus*. *Appl. Environ. Microbiol.* **79**, 2218–2224 (2013).
25. P. J. H. Scott, X. Shao, Fully automated, high yielding production of *N*-succinimidyl 4-[^{18}F] fluorobenzoate ([^{18}F]SFB), and its use in microwave-enhanced radiochemical coupling reactions. *J. Label. Compd. Radiopharm.* **53**, 586–591 (2010).
26. M. Nahrendorf, E. Keliher, B. Marinelli, P. Waterman, P. F. Feruglio, L. Fexon, M. Pivovarov, F. K. Swirski, M. J. Pittet, C. Vinegoni, R. Weissleder, Hybrid PET-optical imaging using targeted probes. *Proc. Natl. Acad. Sci. U.S.A.* **107**, 7910–7915 (2010).
27. R. W. Davis IV, A. D. Brannen, M. J. Hossain, S. Monsma, P. E. Bock, M. Nahrendorf, D. Mead, M. Lodes, M. R. Liles, P. Panizzi, Complete genome of *Staphylococcus aureus* Tager 104 provides evidence of its relation to modern systemic hospital-acquired strains. *BMC Genomics* **17**, 179 (2016).

28. N. Green, H. Alexander, A. Olson, S. Alexander, T. M. Shinnick, J. G. Sutcliffe, R. A. Lerner, Immunogenic structure of the influenza virus hemagglutinin. *Cell* **28**, 477–487 (1982).
29. G. Kohler, C. Milstein, Derivation of specific antibody-producing tissue culture and tumor lines by cell fusion. *Eur. J. Immunol.* **6**, 511–519 (1976).
30. V. T. Oi, L. A. Herzenberg, Immunoglobulin-producing hybrid cell lines, in *Selected Methods in Cellular Immunology*, B. B. Mishell, S. M. Shigi, Eds. (Freeman, 1980), pp. 351–371.
31. P. Panizzi, R. Friedrich, P. Fuentes-Prior, H. K. Kroh, J. Briggs, G. Tans, W. Bode, P. E. Bock, Novel fluorescent prothrombin analogs as probes of staphylocoagulase-prothrombin interactions. *J. Biol. Chem.* **281**, 1169–1178 (2006).

Acknowledgments: For help with radiochemistry, we acknowledge H.-Y. Kim at Massachusetts General Hospital and R. Jackson, J. Mroz, G. Yoon, and J. Baquero at the Bernard and Irene Schwarz Center for Biomedical Imaging, New York University, New York, NY, USA. We thank J. Bose of University of Kansas Medical Center for providing *S. aureus* bacteria. **Funding:** This work was funded in part by grants from the NIH (HL139598, HL114477, HL131495, HL071544, HL130018, CA220234, HL144072, HL131478, EB017183, and NWO/ZonMW Vici 91818622), the American Heart Association (16SDG30190009 and 16POST27030023), the Deutsche Forschungsgemeinschaft (KR4613/1-1), and the MGH Research Scholar Program.
Author contributions: P.P., M.K.-G., Y.-X.Y., J.G., V.F., and Y.S. induced endocarditis in mice, imaged mice, harvested tissues, performed in vitro assays, and analyzed data. P.P., E.K., and M.N. invented the imaging probes that were made and validated by E.K. Y.I. performed mouse and pig histology. G.R.W. did optical imaging, PET/CT, and MRI in mice. G.Courties, M.K.-G., and Y.-X.Y. did intravital microcopy in mice. P.P., S.B., G.H., K.P.R., B.A., P.H.W., D.M.T., F.K.S., and M.N. conceived, developed, and characterized the piglet endocarditis model. Pig endocarditis was induced and imaged by P.P., C.G.M., M.M.T.v.L., A.Meerwaldt, Y.C.T., J.M., A.Maier, G.S., C.C., C.P.-M., G.Carlucci, K.P.R., S.B., G.H., B.A., A.M.-A., I.M.V., P.E.B., P.H.W., D.M.T., and W.J.M.M. K.B., A.M.-A., I.M.V., P.E.B., and W.R.C. developed and characterized immunotherapy. All results were analyzed and discussed by P.P., M.K.-G., F.K.S., and M.N. P.P. and M.N. conceived, designed, and directed the study. M.N., P.P., M.K.-G., E.K., Y.-X.Y., J.G., and W.J.M.M. wrote the manuscript, which was revised and approved by all authors. **Competing interests:** P.P., E.K., and M.N. are inventors on a provisional patent application (63/045,234) submitted by Massachusetts General Hospital that covers a PET and optical imaging agent for endocarditis and clotting. W.R.C. is an inventor on U.S. patent (US 2018/0371108 A1) submitted by Green Mountain Antibodies for an antibody that detects and therapeutically blocks staphylocoagulase. K.B. is an employee of Green Mountain Antibody, and W.R.C. is the owner of Green Mountain Antibody. All other authors declare that they have no competing interests. M.N. has received consulting fees unrelated to this work from Verseau, Gimv, and IMF Therapeutics. F.K.S. has received consulting fees unrelated to this work from Verseau. **Data and materials availability:** All data associated with this study are available in the paper or the Supplementary Materials.

Submitted 30 May 2019
Resubmitted 05 May 2020
Accepted 16 September 2020
Published 4 November 2020
10.1126/scitranslmed.aay2104

Citation: P. Panizzi, M. Krohn-Grimberghe, E. Keliher, Y.-X. Ye, J. Grune, V. Frodermann, Y. Sun, C. G. Muse, K. Bushey, Y. Iwamoto, M. M. T. van Leent, A. Meerwaldt, Y. C. Toner, J. Munitz, A. Maier, G. Soultanidis, C. Calcagno, C. Pérez-Medina, G. Carlucci, K. P. Riddell, S. Barney, G. Horne, B. Anderson, A. Maddur-Appajaiah, I. M. Verhamme, P. E. Bock, G. R. Wojtkiewicz, G. Courties, F. K. Swirski, W. R. Church, P. H. Walz, D. M. Tillson, W. J. M. Mulder, M. Nahrendorf, Multimodal imaging of bacterial-host interface in mice and piglets with *Staphylococcus aureus* endocarditis. *Sci. Transl. Med.* **12**, eaay2104 (2020).

Science Translational Medicine

Multimodal imaging of bacterial-host interface in mice and piglets with *Staphylococcus aureus* endocarditis

Peter PanizziMarvin Krohn-GrimbergheEdmund KeliherYu-Xiang YeJana GruneVanessa FrodermannYuan SunCharlotte G. MuseKaitlyn BusheyYoshiko IwamotoMandy M. T. van LeentAnu MeerwaldtYohana C. TonerJazz MunitzAlexander MaierGeorgios SoultanidisClaudia CalcagnoCarlos Pérez-MedinaGiuseppe CarlucciKay P. RiddellSharron BarneyGlenn HorneBrian AndersonAshoka Maddur-AppajaiahIngrid M. VerhammePaul E. BockGregory R. WojtkiewiczGabriel CourtiesFilip K. SwirskiWilliam R. ChurchPaul H. WalzD. Michael TillsonWillem J. M. MulderMatthias Nahrendorf

Sci. Transl. Med., 12 (568), eaay2104. • DOI: 10.1126/scitranslmed.aay2104

Imaging infection

Infection of the lining of the heart and valves (endocarditis) can be difficult to treat, and proper identification of the causal pathogen is very important. Panizzi *et al.* developed small-molecule imaging agents based on dabigatran, a thrombin inhibitor, to visualize *Staphylococcus aureus* endocarditis. Positron emission tomography and intravital microscopy using the imaging agents revealed that treatment with neutralizing antibodies reduced thrombin deposition and impeded *S. aureus* endocarditis growth in mice. The imaging agents could also be used to visualize infections in piglets. These imaging tools could help monitor disease progression and response to treatment.

Science Translational Medicine (ISSN 1946-6242) is published by the American Association for the Advancement of Science. 1200 New York Avenue NW, Washington, DC 20005. The title *Science Translational Medicine* is a registered trademark of AAAS.